Missouri University of Science and Technology

Scholars' Mine

Geosciences and Geological and Petroleum Engineering Faculty Research & Creative Works

Geosciences and Geological and Petroleum Engineering

01 May 2022

Comprehensive Evaluation of Self-Healing Polyampholyte Gel Particles for the Severe Leakoff Control of Drilling Fluids

Lili Yang

Chunlin Xie

Tian Ao

Kaixiao Cui

et. al. For a complete list of authors, see https://scholarsmine.mst.edu/geosci_geo_peteng_facwork/2062

Follow this and additional works at: https://scholarsmine.mst.edu/geosci_geo_peteng_facwork

 Part of the Geological Engineering Commons, and the Petroleum Engineering Commons

Recommended Citation

L. Yang and C. Xie and T. Ao and K. Cui and G. Jiang and B. Bai and Y. Zhang and J. Yang and X. Wang and W. Tian, "Comprehensive Evaluation of Self-Healing Polyampholyte Gel Particles for the Severe Leakoff Control of Drilling Fluids," *Journal of Petroleum Science and Engineering*, vol. 212, article no. 110249, Elsevier, May 2022.

The definitive version is available at https://doi.org/10.1016/j.petrol.2022.110249

This Article - Journal is brought to you for free and open access by Scholars' Mine. It has been accepted for inclusion in Geosciences and Geological and Petroleum Engineering Faculty Research & Creative Works by an authorized administrator of Scholars' Mine. This work is protected by U. S. Copyright Law. Unauthorized use including reproduction for redistribution requires the permission of the copyright holder. For more information, please contact scholarsmine@mst.edu.

Journal of Petroleum Science and Engineering 212 (2022) 110249

Contents lists available at ScienceDirect

Journal of Petroleum Science and Engineering

journal homepage: www.elsevier.com/locate/petrol

Comprehensive evaluation of self-healing polyampholyte gel particles for the severe leakoff control of drilling fluids

Lili Yang [a,*], Chunlin Xie [a], Tian Ao [a], Kaixiao Cui [a], Guancheng Jiang [a,**], Baojun Bai [b], Yongwei Zhang [a], Jun Yang [a], Xingxing Wang [a], Weiguo Tian [c]

[a] MOE Key Laboratory of Petroleum Engineering, State Key Laboratory of Petroleum Resources and Prospecting, China University of Petroleum (Beijing), Changping District, Beijing, 102249, China

[b] Department of Geosciences and Geological and Petroleum Engineering, Missouri University of Science and Technology, Rolla, MO65409, USA

[c] Beijing National Laboratory for Molecular Sciences, CAS Key Laboratory of Engineering Plastics, Institute of Chemistry Chinese Academy of Sciences (CAS), Beijing, 100190, China

ARTICLE INFO

Keywords:
Oil industry
Drilling fluid
Lost circulation
Reservoir damage prevention
Hydrogel
Self-healing

ABSTRACT

Lost circulation has been a serious problem to be solved in many drilling practices during oil, gas and geothermal well drillings. Many materials have been developed and evaluated for the purpose. However, their performance to plug severe leakoff is very limited. Herein, an injectable self-healing hydrogel based on polyampholyte with sulfonated and quaternary ammonium functionalities (P(MPTC-*co*-NaSS)) was developed and comprehensively evaluated to prevent the severe loss of fluids to formation. By incorporating cation-π (π is for aromatic residues) interaction, the hydrogel shown self-healing property and robustness in severe environment (temperature, salt) by comparison with other hydrogels merely consisting of cation-anion and H-bonding interactions. Aromatic residues enhanced thermal stability above 310 °C. The plugging measurement shown that an addition of 2 wt% dried gel particles can plug high-permeability formation and endure a high pressure of 6 MPa, produce much lower circulation loss and result in a dramatically increased loss volume reduction rate (63.5%) compared with a commercial polymer gel product and an inert material (9.4%) after a self-healing process. Markedly, P(MPTC-*co*-NaSS) can be used in a wide range of formation temperature (as high as 150 °C) and salt concentrations (NaCl, $CaCl_2$, as high as 15 wt %). In addition to suitable particle size and mechanically robustness, it was also attributed to the soft, swelling, deformable, toughness and self-healable features of P(MPTC-*co*-NaSS) gel particles as well as the strong adhesion to negatively charged formations in water, even under high thermal and saline condition. These characteristics also contributed to a long-term plugging performance, beneficial to avoid repeated lost circulation in drilling operation. Besides, this self-healing polyampholyte gel particles dispersed well in saline fluid and maintained stable rheological properties after hot rolling, which was favorable to drilling fluid circulation. This study shown the application potential of self-healing materials as plugging material candidate in petroleum drilling industry.

1. Introduction

Drilling operations are the first step for oil and gas exploration and exploitation. To suspend the drilling cuttings and weighting material and stabilize the wellbore, vast drilling fluids have been utilized in oil, gas and geothermal well drillings (Vipulanandan and Mohammed, 2015; Celino et al., 2022; Jiang et al., 2021). Although drilling fluid density has been carefully designed to ensure that the mud weight is lower than the formation fracture resistance, the lost circulation might still occur because of insufficient knowledge about the actual mechanical characteristics. The existence of fissures or fractures in the formation or a highly porous rock matrix surrounding the borehole would aggravate the situation. Severe lost circulation might also induce formation damage and complicated issues involving hole collapses, stuck pipe and loss of well control (Xu et al., 2022; Abbas et al., 2019). Moreover, dealing with these problems could significantly increase nonproductive time (NPT) and therefore lead to an escalated drilling cost. According to a report from the China National Petroleum Corporation in 2017, dealing

* Corresponding author.
** Corresponding author.
E-mail addresses: yangll@cup.edu.cn (L. Yang), m15600263100_1@163.com (G. Jiang).

https://doi.org/10.1016/j.petrol.2022.110249
Received 5 December 2021; Received in revised form 12 January 2022; Accepted 29 January 2022
Available online 2 February 2022
0920-4105/© 2022 Elsevier B.V. All rights reserved.

with lost circulation accounted for 70% of the total time spent on accident treatments in China. It was also reported that the lost circulation problem has given rise to an expenditure of an additional 1 billion dollars each year, and 10–20% of the total cost of drilling high-temperature and high-pressure wells has been expended on drilling fluid losses (Feng et al., 2018). In these circumstances, filtration control additives, a common additive to mitigate fluid penetration, become ineffective to combat the vast drilling fluid leakage for their small size and the inappropriate mechanism (Dias et al., 2015; Yang et al., 2017a). Therefore, effective circulation loss control material is of great significance to the safety and economic benefits of drilling operations.

Various plugging materials have been employed to add into drilling fluids, especially for water-based drilling fluid (WBDF), which can preventatively minimize the occurrence of lost circulation (Cui et al., 2021; Li et al., 2021; Chu et al., 2019; Magzoub et al., 2020) These plugging materials can be classified into inert materials (calcium carbonate, plant fibers, etc.), inorganic cements (sulfoaluminate cements), organic crosslinked polymers and the composites of these materials. However, inert materials cannot form very effective slug due to their weak interactions between the material interfaces, whereas inorganic cements probably face weak cementation problem and probably contaminate drilling fluids due to abundant Ca^{2+} and Mg^{2+}. Polymer-based crosslinked gel plugging materials have been developed by virtue of its compactness (Xie et al., 2021; Al-Muntasheri et al., 2009). However, they cannot be recovered once be damaged, due to the lack of sufficient interactions between material interfaces, which is disadvantageous for preventing lost circulation during drilling. There exists a continuing effort for developing high-performance plugging materials and achieving long-term plugging.

So far, self-healing hydrogel has been fabricated through abundant noncovalent bonds. Noncovalent bonds endow the hydrogel self-healing capability, and thereby high mechanical toughness, fatigue resistance, and other properties. Self-healing hydrogels have attracted extensive attention for their potential applications in numerous fields, such as coatings (Yuk et al., 2016), sealants (Korde and Kandasubramanian, 2020), tissue adhesives (Gao et al., 2018), soft robotics (Xu et al., 2020), tissue engineering (Zhang et al., 2021), and drug delivery (Niamlaem et al., 2020). A few studies have involved the self-healing hydrogel in profile control and water shutoff (Wang et al., 2017a; Liu et al., 2015; Shi et al., 2019). In-situ polyacrylamide-based polymer gels cross-linked by metallic ions, such as Cr^{3+} and Al^{3+}, can prevent drilling fluid entering the high-permeability rocks by a great extent and have been successfully applied as plugging materials in recent years (Syed et al., 2014; Sun et al., 2020). However, it has been reported that the behavior of metallic ion crosslinked gels is easily affected by high salinity and high temperature environment. In addition, these metallic ion cross-linkers are toxic and harmful to environment; even endanger the health of human. Therefore, it is particularly interesting and intriguing to investigate whether other self-healing materials are more applicable for plugging and how to realize self-healing strategy.

In recent years, various noncovalently cross-linked self-healing hydrogels have been fabricated through synthesis strategies via reversible supramolecular interactions, such as hydrogen bonding (Dai et al., 2015), supramolecular host–guest interactions (Xiong et al., 2020), electrostatic interactions (Jing et al., 2019), metal coordination (Wang et al., 2020), hydrophobic arrangements (Li et al., 2016), and molecular recognition (Xian and Webber, 2020). Considering the cost effectiveness of raw materials, the ease of one-step synthesis process and the environmentally friendly property, polyampholytes based on electrostatic interactions seem to be a promising candidate to mass production for field application (Yang et al., 2020; Rui and Weikai, 2020). Gong et al. pointed that polyampholyte gels are formed only from bulky and hydrophobic ions and successfully synthesized one gel by the copolymerization of 3-(methacryloylamino)propyl-trimethylammonium chloride (MPTC) and p-styrenesulphonate (NaSS) (Sun et al., 2013). Bai et al. also studied this kind of polyampholyte particle gel in enhanced oil recovery below 80 °C and demonstrated the effectiveness in plugging carbonate reservoirs (Wang et al., 2017b). However, considering the severer lost circulation, and much higher formation temperature than 80 °C encountered as drilling depth increases, it deserves to be further studied for drilling fluid. By selecting appropriate ionic monomer combinations, self-healing hydrogels are expected to construct a slug with adequate strength and toughness, and solve the problem of repeated leakage caused by slug failure during drilling.

In this work, a self-healing polyampholyte hydrogel was synthesized though a UV photocatalysis route. Increased temperature and salinity accelerate the self-healing process, which is easily realized downhole. The particle gels can form a strong and tough slug in pore and cracks of sandstone by cooperation with Na-bentonite particles in WBDFs adaptive for strata of varied pore sizes. Through a set of studies on the mechanical properties, microstructure, and self-healing mechanism of hydrogels, we have revealed the process of self-healing hydrogel sealing the lost formations. Such self-healing hydrogel shows great potential in petroleum drilling as lost control material and also serves as a guide to water shut-off purpose.

2. Experimental

2.1. Materials

4-Styrenesulfonic acid sodium salt (NaSS, 90%), 3-methacrylamido-N,N,N-trimethylpropan-1-aminium chloride (MPTC, 45–55 wt % in deionized (DI) water), 2-oxoglutaric acid (98%), and calcium dichloride (99.99%) were purchased from Aladdin Chemical Reagent Co., Ltd. (Shanghai, China). Sodium carbonate mixture (99%), sodium chloride (99.9%), and Na-bentonite were purchased from Innochem Science & Technology Co., Ltd. (Beijing, China). Quartz sand disks with 5–180 D permeability was purchased from Chuangmeng Instrument Co., Ltd. (Qingdao, China).

2.2. Preparation of P(MPTC-co-NaSS) hydrogel

A hydrogel was synthesized via a photoinitiated polymerization method. In detail, a certain amount of MPTC, NaSS, DI water, and photoinitiator 2-oxoglutaric acid were added into a three-necked flask. The mixture was stirred with mechanical agitation and heated to 37 °C in a nitrogen atmosphere until complete dissolution was achieved. Subsequently, the solution was poured into a polytetrafluoroethylene mold prepared in advance and immediately irradiated with 365 nm UV light at a light intensity of 35 mw/cm^2 for 24 h. The resulting product was a transparent hydrogel and nominated as P(MPTC-*co*-NaSS) hydrogel in this study.

The as-prepared hydrogel was dried in an oven at 70 °C for 24 h and then crushed into particles using a high-speed multifunctional crusher. Particles with a mesh size of 40–100 were selected for subsequent studies.

2.3. Plugging performance in WBDF

The blended P(MPTC-*co*-NaSS) particle gels mentioned above was used for the following plugging performance and rheological properties study. A high-temperature and high-pressure (HTHP) GGS71-A fluid loss instrument (Tongchun, China) was employed to evaluate the ability of hydrogel particles to plug and block a permeable sand disk at temperatures of 70, 90, 110, 130 and 150 °C. The pressure was increased 1 MPa every 2 min, and the corresponding fluid losses were recorded. The fluid loss volume measured immediately when the experiment began was defined as the instantaneous leakage volume (V_0), while the latter measured fluid loss volume was defined as the first cumulative leakage volume (V_1).

A secondary plugging experiment was subsequently carried out. After V_1 was determined, the pressure was reduced to 1 MPa. After a few

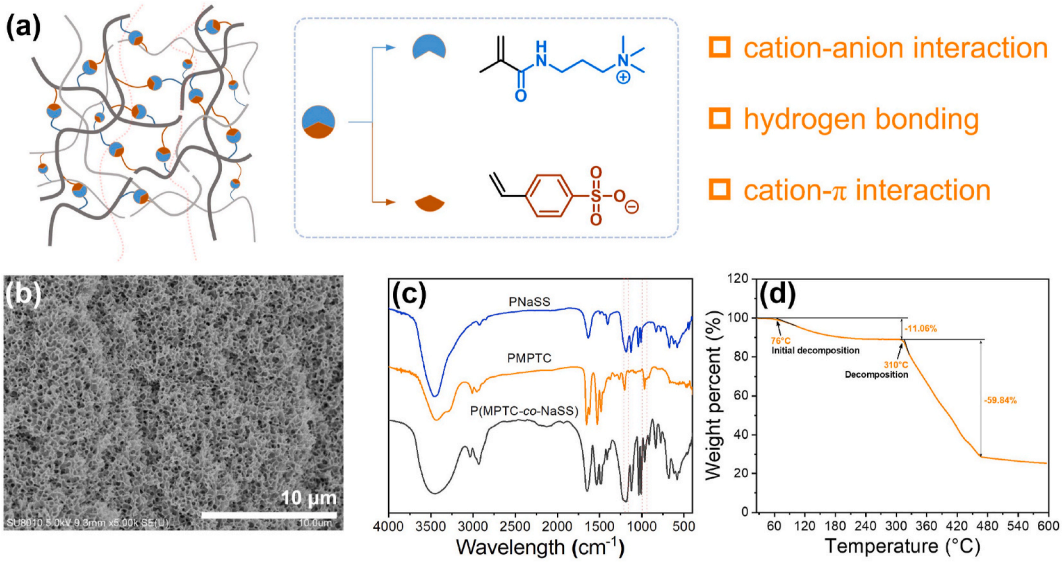

Fig. 1. (a) Schematic illustration of P(MPTC-*co*-NaSS) hydrogel crosslinked by dynamic cation-π interaction, cation-anion interaction and hydrogen bonding; (b) SEM photograph of P(MPTC-*co*-NaSS) hydrogel; (c) FTIR spectra of PMPTC, PNaSS and P(MPTC-*co*-NaSS); (d) thermal stability of P(MPTC-*co*-NaSS).

hours, the fluid loss volume, was measured again and recorded in the same way as V_1, and defined as the secondary cumulative leakage volume (V_2). The leakage volume reduction rate (LVRR) of the sand disk was calculated as follows to quantitatively analyzing the plugging performance of hydrogel particles:

$$\mathrm{LVRR} = \frac{V_1 - V_2}{V_1} \tag{1}$$

The sand disk porosity before and after plugging was measured by a nano-Voxel 4000 high-resolution X-ray three-dimensional micro-CT (Tianjing Sanying, China) at a test tube voltage of 200 kV, a tube current of 300 μA and a resolution of 23.87 μm.

The salinity tolerance of WBDF was measured by adding NaCl and $CaCl_2$ into WBDF at a wide concentration range (2.5–15 wt %) at 90 °C, and the secondary plugging experiment was performed after 3 h.

2.4. Characterization of P(MPTC-co-NaSS) hydrogel

2.4.1. Dynamic thermomechanical analysis (DMA) measurement

Dynamic mechanical analysis was performed to evaluate the viscoelasticity of the P(MPTC-*co*-NaSS) hydrogel using DMA Q800 equipment (TA, USA). A rectangular hydrogel sample (dimensions of 11.6 mm × 7.5 mm × 2 mm) was prepared in advance. The test was conducted in single cantilever beam mode with a frequency of 1 Hz in the temperature range from 20 to 120 °C at a heating rate of 3 °C/min.

2.4.2. Thermogravimetric (TGA) analysis

The TGA curve of the dried sample was obtained using the STA 449F5 (Netzsch, Germany) in the temperature range of 20–600 °C at a heating rate of 10 °C·min^{-1} under a N_2 flow.

2.4.3. Fourier transform infrared (FTIR) spectroscopy measurement

The compositions and chemical structure of P(MPTC-*co*-NaSS) hydrogel was determined through FTIR analysis with a Magna-IR 560 spectrometer (Nicolet, USA) in the wavelength range of 400–4000 cm^{-1} at a resolution of 4 cm^{-1}.

2.4.4. Scanning electron microscopy (SEM) observation

P(MPTC-*co*-NaSS) hydrogel was immersed in DI water or NaCl solutions at varying concentrations. After swelling equilibrium was reached, the hydrogel was directly lyophilized to constant weight. The micromorphologies of the surface and cross section of dried gels were observed using an SU8010 SEM (Hitachi Limited, Japan) at an accelerating voltage of 10 kV.

2.5. Salt response measurement

2.5.1. Influence of salinity on mechanical properties of P(MPTC-co-NaSS) hydrogel

P(MPTC-*co*-NaSS) hydrogel used for tensile test was cut into a dumbbell shape with a length of 30 mm, a width of 6 mm, and a thickness of 3 mm. For compression test, a pellet with a diameter of 12 mm and a height of 6 mm was prepared. The prepared hydrogels were soaked in NaCl solutions with different concentrations. After 12 h, the hydrogels were collected, and the water on the surface of the hydrogel was carefully driven away prior to measurement. The tensile and compression tests were completed using a WH-5000 electronic universal testing machine (Ningbo Weiheng, China) at a tensile speed of 120 mm/min and a compression speed of 5 mm/min.

2.5.2. Influence of salt concentration on expansion capacity and light transmittance of P(MPTC-co-NaSS) hydrogel

P(MPTC-*co*-NaSS) hydrogel pellets with a diameter of 12 mm and a thickness of 6 mm were prepared. The pellets were separately immersed in NaCl solutions at varying concentrations for 24 h. Subsequently, each hydrogel pellet was placed on a grid paper to measure its approximate expansion volume and observe the light transmission performance.

2.6. Self-healing performance test

2.6.1. Half-dumbbell hydrogel self-healing test

Two dumbbell-shaped P(MPTC-*co*-NaSS) hydrogels were immersed in DI water and rhodamine solution to obtain white and red color samples, respectively. Subsequently, the gels were cut in half across the middle. The different colored half-dumbbell samples were kept in contact along the cut section, and a mechanical tensile test was performed a few hours later.

2.6.2. Hydrogel particle reconstruction test

P(MPTC-*co*-NaSS) particle gels with mesh sizes of 40–60 and 60–100 were blended and put into a syringe at a ratio of 1:1. After static setting for 2 d, the excess water in the needle tube was drained, and the formed gel in the syringe was collected for the mechanical compression test.

2.7. Rheological performance in WBDF

Na-bentonite base fluid was prepared at a concentration of 4 wt % in advance. Subsequently, 2 wt % gel particles and NaCl at varied concentrations were added to the base fluid, and then a ZNN-D6B electric six-speed viscometer (Tongchun, China) was utilized to assess the rheological properties. For comparison, the base fluid was also measured as a control. The formula for calculating the rheological parameters of the drilling fluid are as follows (Yang et al., 2017b):

$$AV = \theta_{600}/2 \tag{2}$$

$$PV = \theta_{600} - \theta_{300} \tag{3}$$

$$YP = 0.511(\theta_{300} - PV) \tag{4}$$

where AV is the apparent viscosity of WBDF, mPa·s; PV is the plastic viscosity of WBDF, mPa·s; and YP is the yield point of WBDF, Pa.

The rheological performance of drilling fluid as a function of temperature and pressure was determined by a Fann iX77 rheometer (Fann, USA). The WBDF was stirred at 10,000 rad/min for 20 min in advance. The rheological measuremnts were performed at a set of temperatures and pressures.

3. Results and discussion

3.1. Characterization of P(MPTC-co-NaSS)

A series of hydrogels were synthesized by changing molar ratios of MPTC and NaSS (MPTC/NaSS ratio) (Fig. 1). When the total monomer concentration is over 1.0 mol/L, a hydrogel was formed near an equimolar ratio (Figure S1a and S1c and S1d). It was also found that NaSS was allowed to be added at a slightly higher ratio, for example, a MPTC/NaSS ratio of 3/7 (Figs. S1c and S1d). Herein, A P(MPTC-*co*-NaSS) hydrogel formed at a total monomer concentration of 2 mol/L and a MPTC/NaSS ratio of 5/5 was selected for following study (Sun et al., 2013). As depicted in the FTIR spectra (Fig. 1b), the peaks corresponding to phenyl ring, sulfonate, and quaternary ammonium group marginally blue shifted from 1406, 1184 and 965 cm^{-1} in PMPTC and PNaSS homopolymers to 1410, 1186, and 966 cm^{-1} in P(MPTC-*co*-NaSS), respectively. These small shifts indicate the formation of intrachain and interchain noncovalent interactions between phenyl, sulfonate, and quaternary ammonium salts (Yang et al., 2005; Jiang et al., 2013; Karthik, 2009). From the SEM photographs (Fig. 3c), a dense, porous, three-dimensional network structure was observed, demonstrating that a stable supramolecular network structure was generated inside the hydrogel.

Some self-healing hydrogels may not be suitable for plugging purpose. As shown in Fig. S2, a hydrogen bond-based hydrogel, poly(N-acryloyl glycinamide) (PNAGA), become a sol or even solution at high temperatures. When MPTC was copolymerized with 2-acrylamido-2-methylpropane sulfonic acid (AMPS), a copolymer (P(MPTC-*co*-AMPS) based on pure ionic bond was prepared. The electrostatic interaction, however, normally diminishes due to Debye screening effect in saline water, especially at high ionic-strength conditions. Incorporation of a styrene sulfonate moiety can enhance the robustness of the hydrogel by forming cation-π (π is for aromatic composition from NaSS monomer) interactions, which is in consistence with adjacently located amino acids of cationic and aromatic residuals in biological systems (Fan et al., 2019). At high temperatures, pure electrostatic interaction is weakened as well because of increased kinetic energy (Fig. S1b). The phenyl group in NaSS can endow the macromolecule with sufficient thermal stability (Mohamed et al., 2021). P(MPTC-*co*-NaSS) shows a higher tensile strength than P(MPTC-*co*-AMPS) (and S3). As shown in Fig. 1c, the initial decomposition temperature of P(MPTC-*co*-NaSS) reaches 310 °C, showing sufficient thermal stability for most field applications.

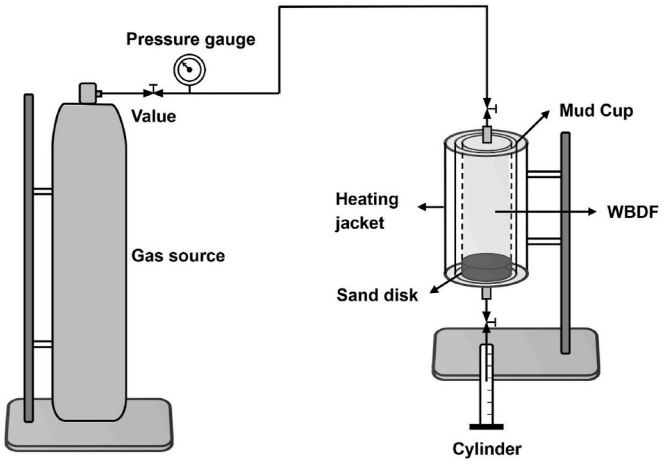

Fig. 2. Schematic diagram of the high-permeability sand disk plugging experiment for WBDF.

3.2. Plugging performance of P(MPTC-co-NaSS) gel particles in WBDF

3.2.1. Comparison between P(MPTC-co-NaSS) gel particles and other commercial products

Considering the requirements for transportation into wellbores and sealing abundant natural and artificial micropores and cracks in formations, particle gels were fabricated. Particle gels were utilized for all following plugging performance evaluations unless indicated otherwise.

The plugging performance was evaluated by means of the instrument with a schematic diagram shown in Fig. 2. The pressure was controlled by a gas source. After a traditional plugging evaluation, the differential pressure was reduced to 1 MPa for a period before a second measurement to accomplish self-healing process. By observing a sand disk with an original permeability of 180 D before and after plugging through the X-ray CT technique, we found that the average porosity was markedly dropped from 9.86% to 1.06%, by a reduction rate of 90% (Fig. 3a and b). The pore space (shown in blue) was reduced and plugged (shown in white). After the sand disk was recollected and dried, a connected structure was observed, showing strong adhesion affinity to negatively charged surface. These results indicate that P(MPTC-*co*-NaSS) gel particles can pronouncedly decrease the porosity of high permeability formations.

To further illuminate the plugging performance of P(MPTC-*co*-NaSS) gel particles, commercial polymer gel particles and an inert material (mixture of nut shells and $CaCO_3$ particles) of similar size were also evaluated (Fig. 3c and d). Compared with pure Na-bentonite fluid, the instantaneous leakage volume V_0 was reduced from almost the total volume to 17.0, 24.0, and 40.0 ml, respectively, which indicated that all three materials are capable of bridging and blocking pores. Notably, the healable P(MPTC-*co*-NaSS) gel particles performed the best. After the initial plug was formed, the first cumulative leakage volume V_1 was reduced to 31.5, 32.0, and 40.0 ml as the pressure was increased successively from zero to 6 MPa over 12 min. This indicated that the proposed P(MPTC-*co*-NaSS) gel particles and the commercial gel particles form a compacter packing in the pores compared to inert material. Specifically, the P(MPTC-*co*-NaSS) gel particles shown a better ability to mitigate leakage than the commercial hydrogel product for the instantaneous and first filtration stages. After the pressure was reduced to 1 MPa for an hour, it was applied again to start the second cumulative leakage stage. The leakage volume in this stage (V_2) was 11.5, 29.0, and 39.0 ml, respectively. It can be seen that P(MPTC-*co*-NaSS) gel particles were able to construct a strong, firm, and dense sealing compared with the other two materials. The loss volume reduction rate (LVRR) reached 63.5%, 9.4%, and 2.5%, respectively, demonstrating that the P(MPTC-*co*-NaSS) gel particles formed a compact bulk gel through its superior

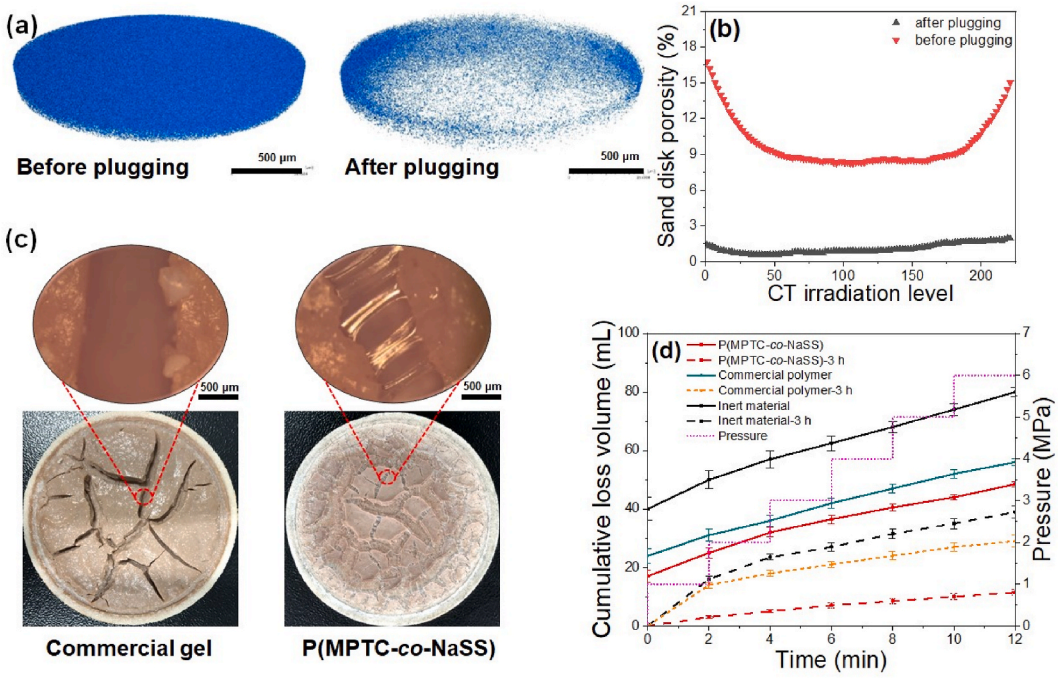

Fig. 3. (a) Reconstructed 3D image of sand disk before and after plugging by P(MPTC-*co*-NaSS) gel particles; (b) Layer porosity distribution of the sand disk before and after plugging based on X-ray CT results; (c) Surface microstructure of freshly prepared sand disk after being plugged by commercial polymer gel particles and P(MPTC-*co*-NaSS) particle gels and the corresponding microstructure of the produced cracks dried at ambient temperature for 1 d; (d) Cumulative loss volume as a function of time for P(MPTC-*co*-NaSS) gel particles, commercial polymer gel particles and inert material, respectively.

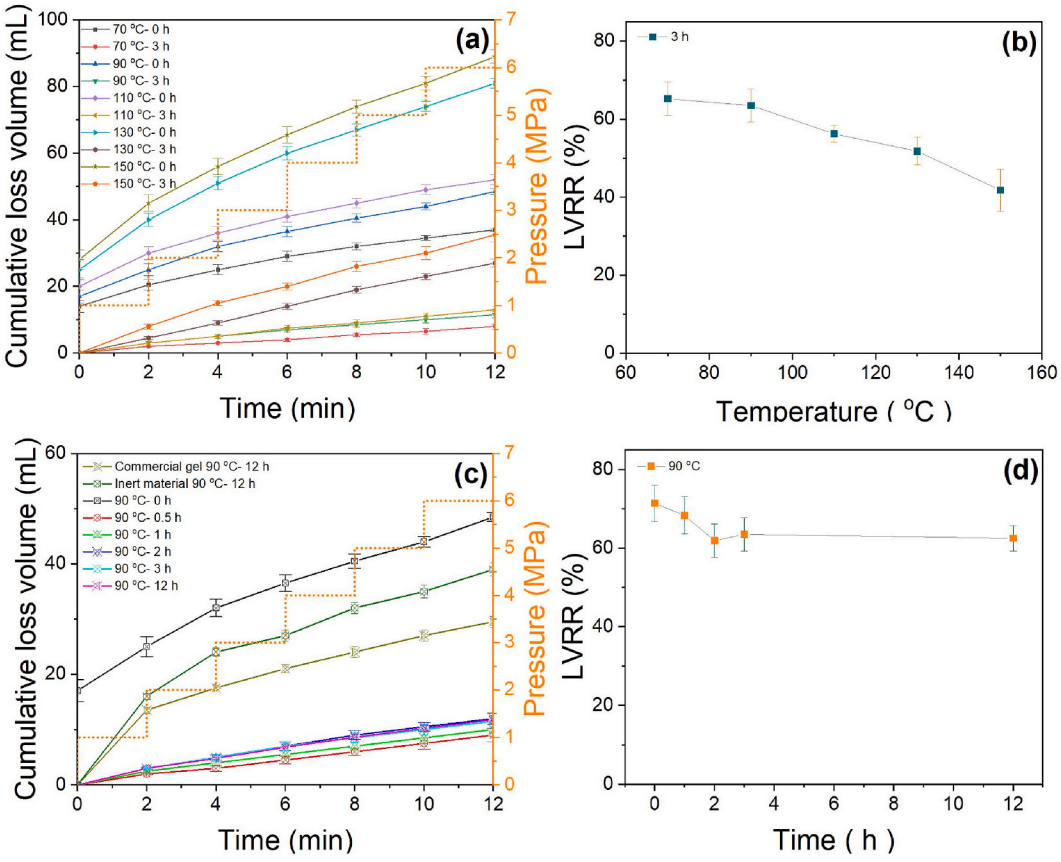

Fig. 4. (a) Cumulative loss volume (V_0, V_1, and V_2) and (b) LVRR of P(MPTC-*co*-NaSS) gel particles at different temperatures, in which V_2 is measured after self-healing for 3 h; (c) Cumulative loss volume (V_0, V_1, and V_2) and (d) LVRR of P(MPTC-*co*-NaSS) gel particles after self-healing for different times at 90 °C.

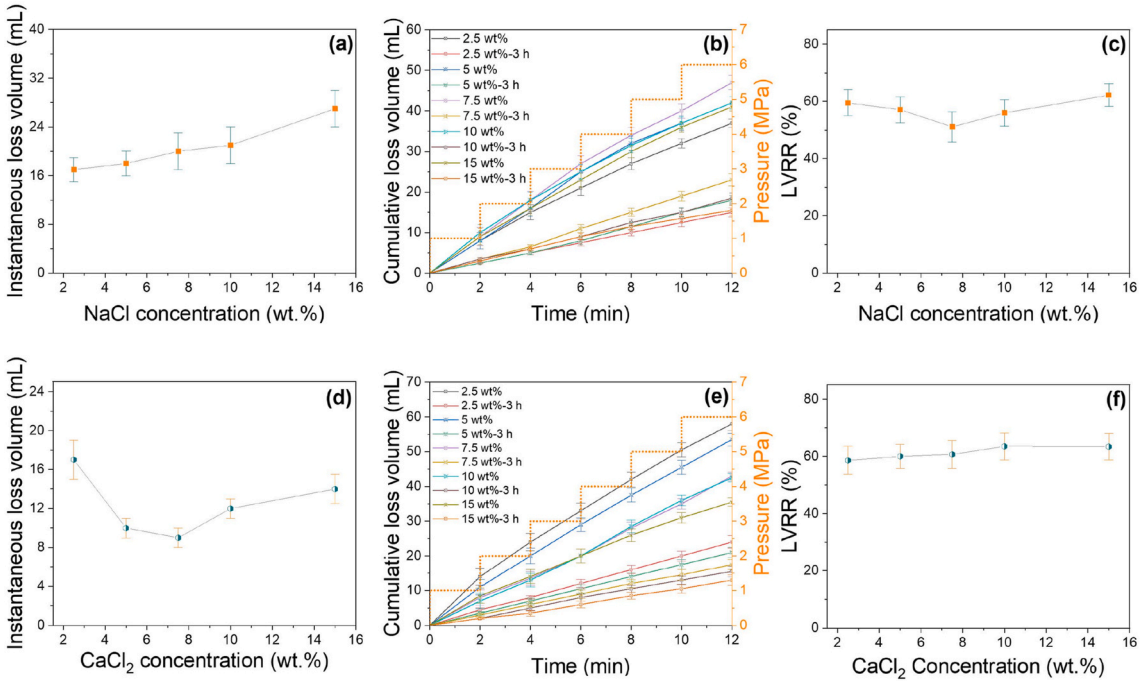

Fig. 5. (a) V_0, (b) V_1 and V_2, and (c) LVRR of P(MPTC-*co*-NaSS) gel particles at different NaCl concentrations; (d) V_0, (e) V_1 and V_2, and (f) LVRR of P(MPTC-*co*-NaSS) gel particles at different $CaCl_2$ concentrations. All tests were conducted at 90 °C, and V_2 was measured after self-healing for 3 h.

self-healing properties. It was also verified by the observation of a merged gel using an optical microscope (Fig. S4). It is also concluded that a reduced differential pressure can promote particles self-healing, probably because that it facilitate the recontact between each other and reabsorption onto the sand, which was operable in field application.

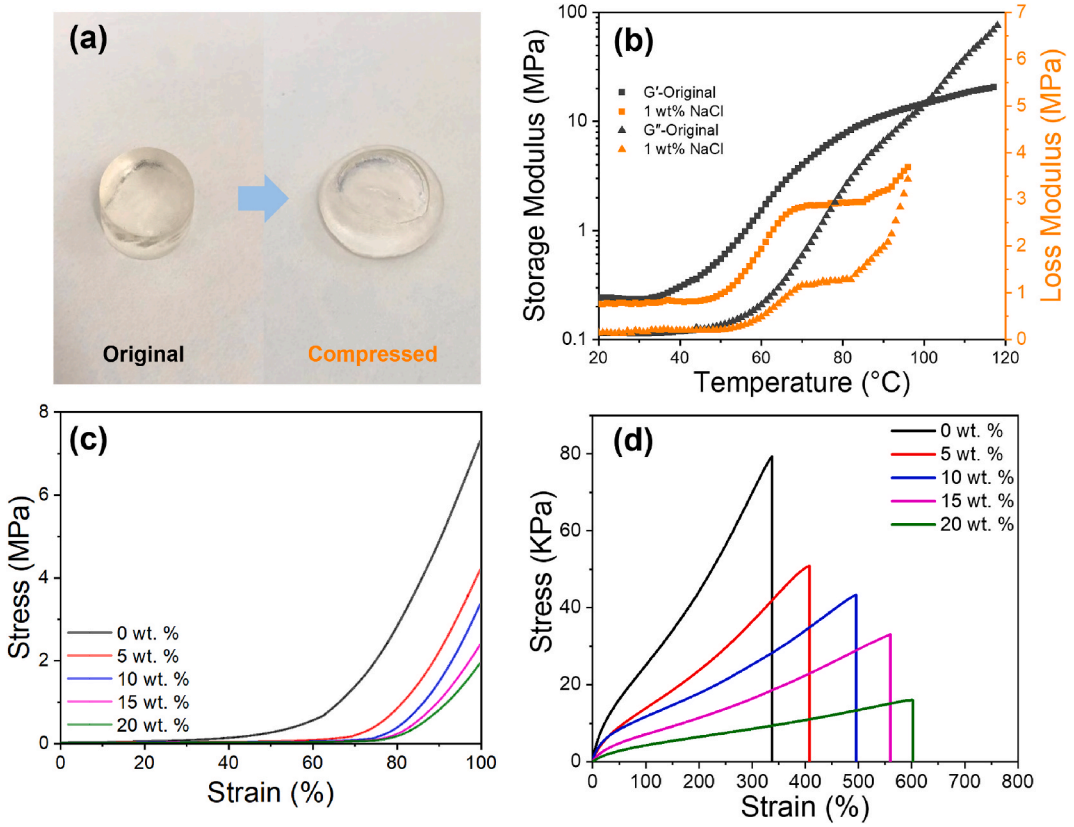

Fig. 6. (a) Photographs showing the high elasticity of hydrogel; (b) Storage moduli and loss moduli of hydrogel as a function of temperature; (c–d) compressive and tensile stress–strain curves of P(MPTC-*co*-NaSS) hydrogels soaked in saline solutions at varied concentrations.

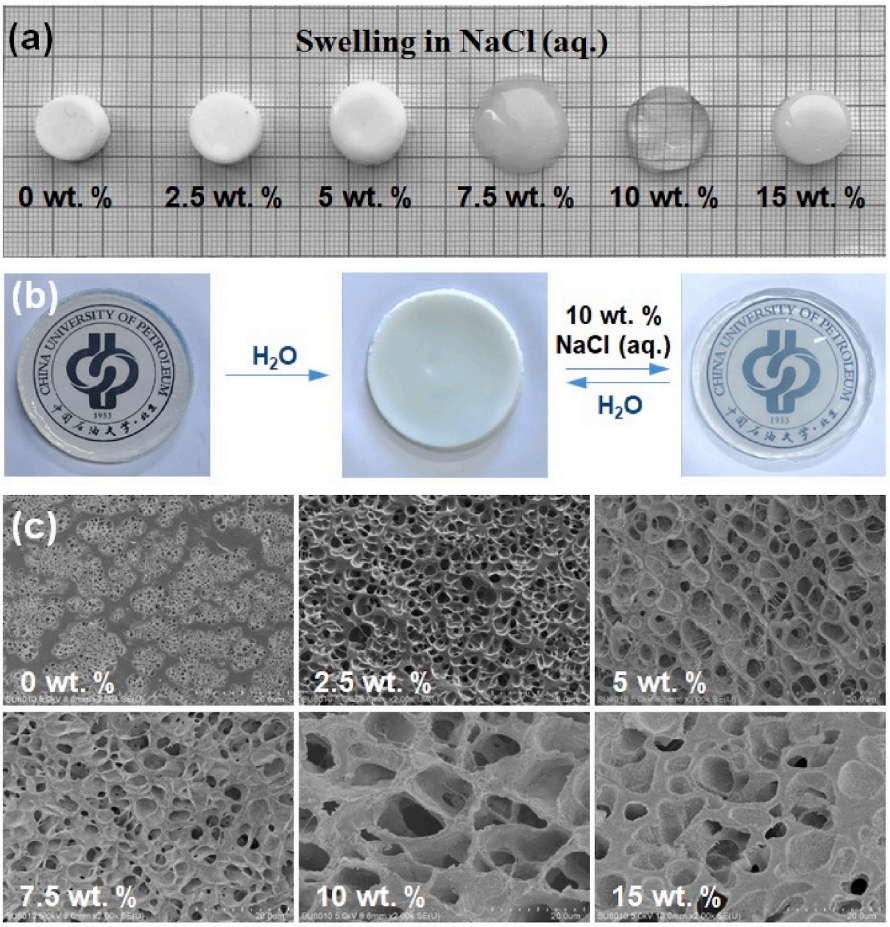

Fig. 7. (a) Swelling of P(MPTC-*co*-NaSS) hydrogel in saline solutions at varied concentrations; (b) Light transmittance of P(MPTC-*co*-NaSS) hydrogel that was freshly prepared, soaked in DI water and 10 wt% NaCl solution, respectively; (c) SEM images of P(MPTC-*co*-NaSS) hydrogels in saline solutions at varied concentrations. The scale in (c) is 20 μm.

3.2.2. *Influence of temperature on the plugging ability of P(MPTC-co-NaSS) gel particles*

To explore the adaptiveness of P(MPTC-*co*-NaSS) gel particles to high temperature and salinity condition, we carried out a series of plugging experiments at temperatures of 70, 90, 110, 130, and 150 °C. Remarkably, it can withstand a pressure of 6 MPa, even in a 150 °C environment. The experimental results (Fig. 4a) show that V_0, V_1, and V_2 were increased from 14 to 28 ml, 23–61 ml, and 8–35.5 ml, with increasing temperature from 70 to 150 °C, respectively. The LVRR values (Fig. 4b) are 65.2%, 63.5%, 56.3%, 51.8%, and 41.8%, respectively.

The long-term effectiveness of P(MPTC-*co*-NaSS) gel particle plugging was evaluated by measuring V_2 after different time intervals (0.5 h, 1 h, 2 h, 3 h, and 12 h). We found that the plugging ability of P(MPTC-*co*-NaSS) gel particle slightly decreased in the first 2 h and then remained constant; the corresponding V_2 values were 9.0, 10.0, 12.0, 11.5, and 11.8 ml (Fig. 4c), respectively. Additionally, the LVRR was calculated to be 71.4%, 68.3%, 61.9%, 63.5%, and 62.5% (Fig. 4d), respectively. Therefore, the plugging efficiency of the self-healing hydrogel on the sand disk remained approximately 63% at 90 °C, indicative of that P(MPTC-*co*-NaSS) gel particle plugging was effective for long-term drilling purposes.

3.2.3. *Influence of salinity on the plugging ability of P(MPTC-co-NaSS) gel particles*

During the drilling process, high salinity, especially high-calcium formations are often encountered, which can lead to a sudden increase in the salinity of the drilling fluid, further affecting its performance. To explore the plugging performance of P(MPTC-*co*-NaSS) gel particles under high saline conditions, we measured V_0, V_1, and V_2 over a wide concentration range (2.5–15 wt %) of NaCl and $CaCl_2$.

The results (Fig. 5 a-c) shown that with the increase in NaCl concentration, V_0 gradually increased from 17.0 ml to 27.0 ml, while V_1 and V_2 first increased and then decreased, reaching maximum values of 47.0 ml and 23.0 ml at a concentration of 7.5 wt %, respectively. The LVRR exhibited the opposite trend, reaching a minimum value of 51.1% when the concentration of NaCl was 7.5 wt %. When the saline solution was replaced by $CaCl_2$ solution (Fig. 9 d-f), as the $CaCl_2$ concentration increased, V_0 first decreased and then increased, reaching a minimum value of 9.0 ml when the concentration of $CaCl_2$ was 7.5 wt %. V_1 and V_2 both gradually decreased from 58.0 to 35.5 ml and 24.0–13.0 ml, respectively, and the LVRR increased from 58.6% to 63.4%. The results shown that P(MPTC-*co*-NaSS) gel particles still maintained excellent plugging performance when the concentration of NaCl and $CaCl_2$ increased to 15 wt %, which suggested that P(MPTC-*co*-NaSS) gel particles possessed extraordinary salt tolerance when used as a plugging material.

3.3. *Plugging mechanism analysis*

The plugging performance was directly related to mechanical properties and swelling ability, according to previous reports. As for P(MPTC-*co*-NaSS) gel particles, self-healing process was also considered since a lowering pressure for a period improved the plugging performance, which was attributed to its self-healing capacity. Bulk hydrogel

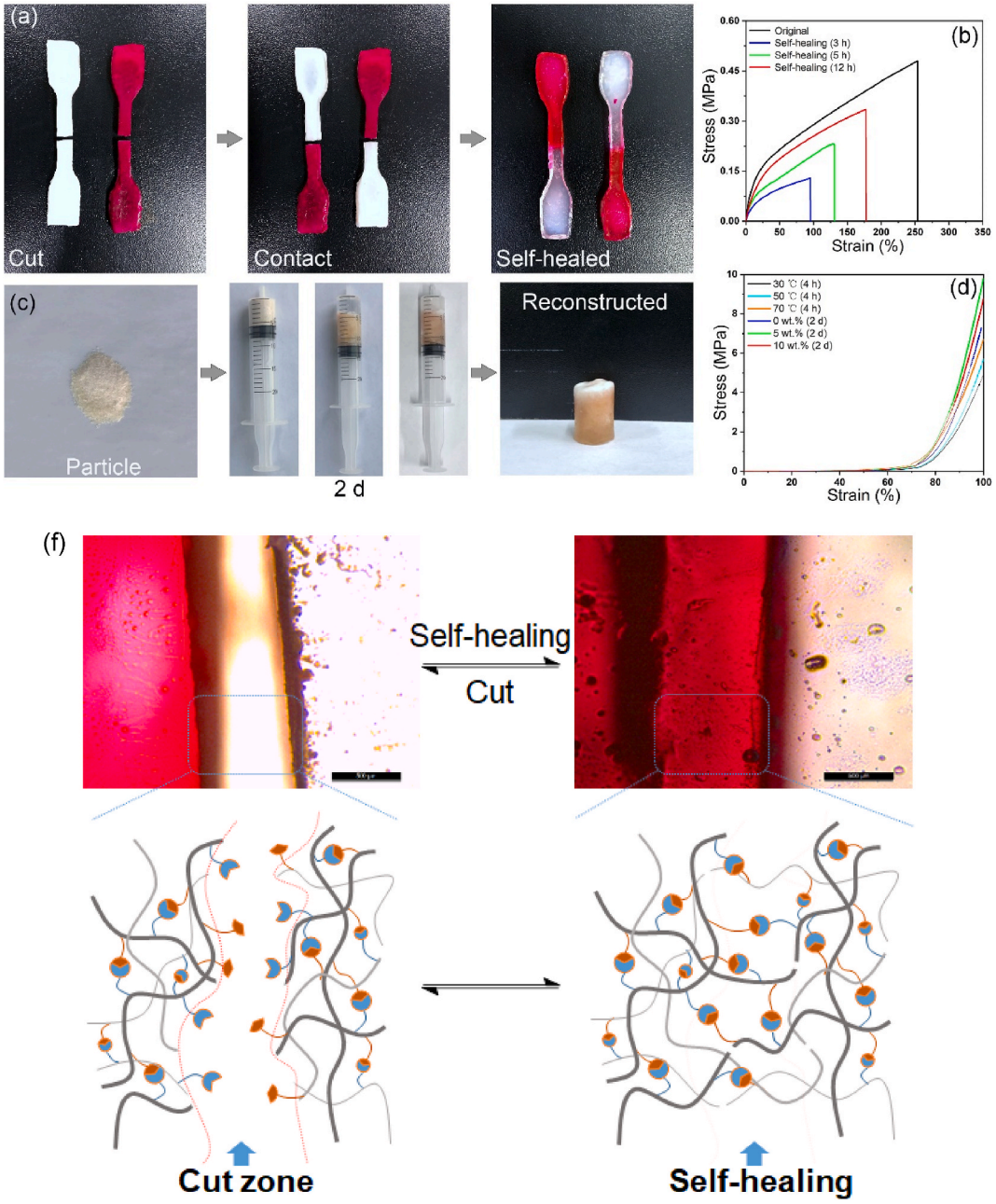

Fig. 8. (a) Self-healing between two freshly cut surface of P(MPTC-*co*-NaSS) hydrogel; (b) Body reconstruction process of P(MPTC-*co*-NaSS) gel particles in NaCl solutions; c) Tensile-testing curves of original and self-healed hydrogel in (a); d) Compressive-testing curves of reconstructed hydrogel in (b); (e) optical photograph of.

might be employed instead of gel particles in some measurements.

3.3.1. *Mechanical properties of P(MPTC-co-NaSS) hydrogel*

P(MPTC-*co*-NaSS) hydrogel was able to withstand compression deformation at room temperature and restore its original shape immediately when the pressure was removed (Fig. 6a), indicative of its highly elastic nature. The considerable elasticity allowed the hydrogel to deform flexibly, enter pores and fractures easily, and then gently regain its original shape. The hydrogel exhibited reversible self recovery performance, which was attributed to rubber-like entropy elastic deformation. When the polymer molecular chain changed from a curled state to a stretched state under external force, its entropy was reduced. Once the external force was removed, the molecular chain spontaneously adopted a state of increased entropy due to thermal movement and returned to the curled state, thereby returning the hydrogel to its original shape. Therefore, the P(MPTC-*co*-NaSS) hydrogel was a highly elastic and shape memory material at room temperature.

The performance of P(MPTC-*co*-NaSS) hydrogels at high temperatures was of even greater concern considering the high-temperature wellbore environment. From the DMA test results, the G′ and G″ of the self-healing hydrogel were found to increase as the temperature increased in the range of 20–120 °C (Fig. 2c). Within the temperature range of 25–100 °C, the G′ values increased to 14.6 MPa from 0.24 MPa, rising most dramatically above 57 °C. It suggested that dynamic cation-π crosslinking were generated by heating, since H-bonding, cation-anion, and dipole-dipole interactions tend to diminish at elevated temperatures. These phenomena illustrated the enhanced thermal stability of the cross-linked network of the P(MPTC-*co*-NaSS) hydrogel at high temperatures, which is advantageous to deal with the lost circulation in high temperature deep well. When the hydrogel specimen was immersed in 1

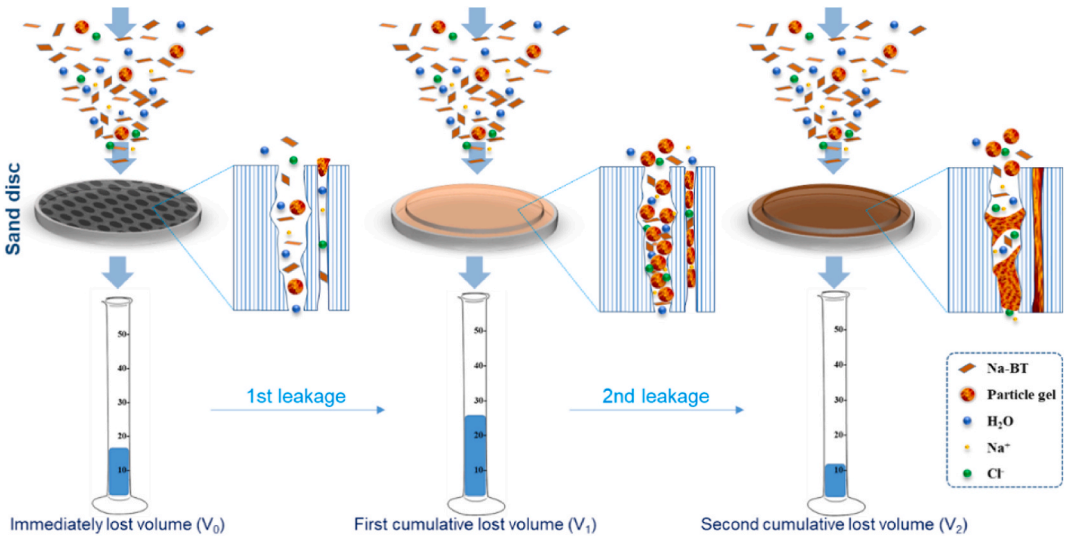

Fig. 9. Evolution of P(MPTC-*co*-NaSS) gel particles in plugging process.

wt % NaCl solution, the G′ and G″ curves adopted the similar trends as that in DI water, despite of reduced G′ and G″ and a decreased transformation temperature (96 °C). Further increase in salt concentration would aggravate the phenomena. A potential explanation for this result was that the bonds of the internal structure were discounted due to the Debye shielding effect and Na^+ competing with polycations to bind with phenyl groups in the hydrogel.

The compressive strength and tensile strength of P(MPTC-*co*-NaSS) hydrogel were further quantitatively assessed by immersing in 0, 5.0, 10.0, 15.0 and 20.0 wt % NaCl solutions (Fig. 6c and d). The compressive strength and tensile strength decreased from 7.3 to 1.9 MPa and 80.0– 16.0 KPa, respectively. The hydrogel can bear deformation with a strain of up to 600%, showing a much higher elongation rate at fracture after soaking in 20.0 wt % NaCl solution. It can be seen the robustness of P(MPTC-*co*-NaSS) hydrogel was decreased, but the toughness was increased on the contrary. Mechanical properties play a key role in achieving efficient plugging.

3.3.2. *Swelling ability and microstructure of P(MPTC-co-NaSS) hydrogel in saline solution*

An increase in the total volume of the hydrogel was observed for P (MPTC-*co*-NaSS) hydrogel immersed in saline solutions at a concentration less than 10.0 wt % (Fig. 7a and b). Final swelling ratio depended on the salinity. Notably, volume swelling was observed as the salt concentration increased from zero to 5 wt %. The theoretically concentration of NaCl existed in the product was approximately 5.8 wt %, and water in the external environment entered the hydrogel because of osmotic pressure and promoted volume swelling by absorbing water. The hydration functionalities also contributed to the total swelling ratio. It was verified when the hydrogel in 7.5 wt % salt solution swelled to twice its original volume, although osmotic pressure mildly inhibited water absorption at this concentration. When the concentration was further increased to 10 wt % and above (15 wt % taken as an example), a decrease in hydrogel volume was observed, indicating that water began escaping from the hydrogel to the external environment because of the significant osmotic pressure.

It was also reflected by the transparency of P(MPTC-*co*-NaSS) hydrogel (Fig. 7b). The in-situ polymerized hydrogel is a homogeneous, transparent gel before soaking, but it gradually whitens after being soaked in DI water or saline solutions at concentrations less than 5.0 wt %. Furthermore, the hydrogel became slightly translucent at a concentration of 7.5 wt %, while the hydrogel recovered homogeneous transparency when the NaCl concentration reached 10 wt % and began shrinking.

The swelling along with transparency reduction as salinity increased can be interpreted by microstructure of P(MPTC-*co*-NaSS) hydrogel. From the SEM results (Fig. 7c), it was found that when the concentration was less than 10 wt %, the pore size and skeleton thickness both progressively increased with increasing salt concentration; when the salt concentration was higher than 10%, the gel shrunk, the pore size decreased, and the gel skeleton thickness increased continuously. The swelling behavior of plugging material is beneficial to further improvement of plugging performance.

3.3.3. *Self-healing performance of P(MPTC-co-NaSS) hydrogel in saline solution*

The self-healing properties were explored by two approaches. In the first method, two dumbbell-shaped hydrogel plates, one of which dyed red, were cut into half-dumbbell pieces, and two halves with different colors were put back into the original mold and sealed (Fig. 8a). The microscopic observation in Fig. 8e shown the incision of the two hydrogels merged together within several hours. Additionally, the self-healed P(MPTC-*co*-NaSS) hydrogel was able to sustain a large tensile force, which confirmed the significant self-healing of the hydrogels. The tensile strengths were 0.14 MPa, 0.26 MPa, and 0.36 MPa, and the tensile deformation rates were 113%, 153%, and 199% after 3 h, 5 h, and 12 h healing, respectively (Fig. 8b). Compared to the original hydrogel, recovery of stress reached 29.2%, 54.2%, and 75%, and recovery of elongation at breaking reached 44.6%, 60.5%, and 78.7%, respectively. The self-healing mechanism resulted from the reconstruction of ionic bonds and cation-π bonds between two surfaces.

The self-healing ability of P(MPTC-*co*-NaSS) gel particles was accessed by using a syringe as a mold to observe the bulk reconstruction performance (Fig. 8c). After aging for over 4 h, the particle gels held together and formed a bulk hydrogel slug, which plug the syringe tightly. When the temperature was increased from room temperature to 70 °C, the mechanical strength was increased from 4.9 MPa to 6.7 MPa (Fig. 8d). It inferred that heating can accelerate the self-healing process. Increasing salt concentration has the same effect below 5 wt%.

Under high-temperature conditions, the internal self-healing mechanism may involve the accelerated movement of long molecular chains inside the hydrogel along with the faster dissociation of ionic bonds, thereby forming new bonds at the interface faster. Salt solution promoted the dynamic dissociation of P(MPTC-*co*-NaSS) residues on the surface due to shielding effect and accelerated the self-healing process. The saline solution gradually destroyed the weaker and stronger bonds, and new bonds were formed at the interface, facilitating the self-healing process. Thus, P(MPTC-*co*-NaSS) hydrogel processed good self-healing

Table 1
Influence of NaCl concentration on rheological properties of WBDFs added with P(MPTC-*co*-NaSS) gel particles.

$C_{Na\text{-}bentonite}$	$C_{P(MPTC\text{-}co\text{-}NaSS)}$	C_{NaCl}	$\theta_{600}/\theta_{300}/\theta_{200}/\theta_{100}/\theta_6/\theta_3$	AV mPa.s	PV mPa.s	YP Pa
4 wt %	2 wt %	0	20/16/14/12/10/9	10	4	6
4 wt %	2 wt %	0	29/24/22/20/14/13	14.5	5	9.5
4 wt %	2 wt %	2.5	31/26/24/22/16/15	15.5	5	10.5
4 wt %	2 wt %	5	40/36/34/30/24/19	20	4	16
4 wt %	2 wt %	7.5	53/44/40/35/19/10	26.5	9	17.5
4 wt %	2 wt %	10	45/35/29/23/8/6	22.8	10	12.5
4 wt %	2 wt %	15	46/33/26/19/7/5	23	13	10

ability and tough mechanical strength. When salinity was increased, the original electrostatic interaction between quaternary ammonium and sulfonate groups and cation-π interaction between quaternary ammonium and phenyl groups were screened while inorganic cations bnded with phenyl groups instead. This variation can retain the self-healing ability but not mechanical property. When salinity was over 5 wt%, the mechanical strength was greatly weakened. Extending the reconstruction time can strengthen the self-healed hydrogel, which can be considered in practice.

In the humid, hot, and probably saline environment of the wellbore, the internal crosslinked network inside P(MPTC-*co*-NaSS) hydrogel particles would be partially destroyed, causing the deformation and softening of the particle, according to the DMA results (Fig. 2c). Hydrogel particles become easier to enter pores and cracks of irregular shape (Fig. 9). Only a slight decrease in plugging performance was observed with elevating temperature and increasing salinity, probably due to the decrease of mechanical strength. It also gives us enlightenment that the reduction of mechanical strength of the hydrogel can be partially counteracted by the increase of the deformation ability. Accordingly, V_1 and V_2 were observed to first increase and then decrease as Na^+ concentration increases can be interpreted that when the NaCl concentration exceeds 7.5 wt %, the P(MPTC-*co*-NaSS) gel particles are more easily squeezed into the pores of the sand disk, further improving the plugging effect. The plugging performance was not deteriorated when $CaCl_2$ was added instead, showing the adaptiveness of P(MPTC-*co*-NaSS) gel particles to different saline environment. The strong plugging ability are primarily attributed to the swelling, deformation, toughness, and self-healing effects of P(MPTC-*co*-NaSS) gel particles in water. Furthermore, they were also ascribed to the strong adhesion with negatively charged Na-bentonite particles and quartz sands, even in high ionic-strength media. These effects synergistically achieve the goal of effective plugging. The internal structure, based on noncovalent crosslinked ionic bonds and cation-π bonds, can serve as a basis for the reference to design better self-healing plugging materials.

3.4. Rheological properties of WBDF

Drilling fluid plays an essential role in suspending and carrying cuttings and weighing materials. Additives for drilling fluid must not excessively affect the original rheological properties of the drilling fluid. On the other hand, the additives should not increase the viscosity of the drilling fluid too much, or it will increase the power consumption of the mud pump and even stall the pump. Therefore, we studied the influence of plugging materials on the rheology of WBDF. As shown in Table 1, the self-healing hydrogel did not increase the viscosity of WBDF. When NaCl was added at different dosages, only a slight increase in apparent viscosity even at a high concentration, showing its compatibility of P (MPTC-*co*-NaSS) gel particles in saline base fluid for drilling process in field application.

4. Conclusion

In summary, a P(MPTC-*co*-NaSS) hydrogel with self-healing ability was synthesized and innovatively used as plugging material for oil, gas and geothermal drilling. Such polyampholyte hydrogel had outstanding salt adaptability and high-temperature resistance that allowed it to maintain plugging performance even in presence of salinity exceeding 15 wt % and at high temperatures, e.g., 150 °C. P(MPTC-*co*-NaSS) gel particles can be easily transported into formations and rapidly formed a bulk gel adaptive to its surroundings via the synergy of deformation, swelling, robustness, self-healing properties, and adhesion to the formations. Plugging experiments demonstrated that P(MPTC-*co*-NaSS) gel particles performed excellent plugging ability and could significantly reduce the porosity of a high permeability sand disk. Furthermore, by lowering drilling operation pressure, a slug was facially reestablished and shown an enhanced plugging performance than before, far superior to a commercial gel particle and an inert plugging material. In addition, this self-healing hydrogel was nontoxic, and had no significant impact on the rheology of WBDF. Therefore, it is a promising material for intelligent and efficient plugging of high-permeability formations in drilling and water flooding process.

Credit author statement

Lili Yang: Methodology; Supervision; Writing - review, Chunlin Xie: Investigation; Methodology; Writing - original draft, Tian Ao: Investigation, Kaixiao Cui: Methodology, Guancheng Jiang: Project administration; Resources, Yongwei Zhang: Validation, Jun Yang: Methodology, Xingxing Wang: Methodology, Weiguo Tian: Writing - review & editing.

Declaration of competing interest

The authors declare that they have no known competing financial interests or personal relationships that could have appeared to influence the work reported in this paper.

Acknowledgments

We gratefully acknowledge support from the National Natural Science Foundation (Grant No. 51874329), the National Natural Science Innovation Population of China (Grant No. 51821092) and the foundation of China University of Petroleum (Beijing) (Grant No. 2462021YXZZ002).

Appendix A. Supplementary data

Supplementary data to this article can be found online at https://doi.org/10.1016/j.petrol.2022.110249.

References

Abbas, A.K., Bashikh, A.A., Abbas, H., Mohammed, H.Q., 2019. Intelligent decisions to stop or mitigate lost circulation based on machine learning. Energy 183, 1104–1113.
Al-Muntasheri, G.A., Nasr-El-Din, H.A., Al-Noaimi, K., Zitha, P.L.J., 2009. A study of polyacrylamide-based gels crosslinked with polyethyleneimine. SPE J. 14 (2), 245–251.
Celino, K.N., Souza, E.A.d., Balaban, R.d.C., 2022. Emulsions of glycerol in olefin: a critical evaluation for application in oil well drilling fluids. Fuel 308, 121959.
Chu, Y.Y., Song, X.F., Zhao, H.X., 2019. Water-swellable, tough, and stretchable inorganic-organic sulfoaluminate cement/polyacrylamide double-network hydrogel composites. J. Appl. Polym. Sci. 136 (35), 47905.
Cui, K., Jiang, G., Xie, C., Yang, L., He, Y., Shen, X., Wang, X., 2021. A novel temperature-sensitive expandable lost circulation material based on shape memory epoxy foams to prevent losses in geothermal drilling. Geothermics 95, 102145.

Dai, X., Zhang, Y., Gao, L., 2015. A mechanically strong, highly stable, thermoplastic, and self-healable supramolecular polymer hydrogel. Adv. Mater. 27 (23), 3566–3571.
Dias, F.T.G., Souza, R.R., Lucas, E.F., 2015. Influence of modified starches composition on their performance as fluid loss additives in invert-emulsion drilling fluids. Fuel 140, 711–716.
Fan, H.L., Wang, J.H., Tao, Z., Huang, J.C., Rao, P., Kurokawa, T., Gong, J.P., 2019. Adjacent cationic-aromatic sequences yield strong electrostatic adhesion of hydrogels in seawater. Nat. Commun. 10.
Feng, Y., Li, G., Meng, Y., Guo, B., 2018. A novel approach to investigating transport of lost circulation materials in rough fracture. Energies 11 (10), 2572.
Gao, Z., Duan, L., Yang, Y., Hu, W., Gao, G., 2018. Mussel-inspired tough hydrogels with self-repairing and tissue adhesion. Appl. Surf. Sci. 427, 74–82.
Jiang, C., He, H., Jiang, H., 2013. Nano-lignin filled natural rubber composites: preparation and characterization. Express Polym. Lett. 7 (5), 480–493.
Jiang, G., Sun, J., He, Y., Cui, K., Dong, T., Yang, L., Yang, X., Wang, X., 2021. Novel Water-Based Drilling and Completion Fluid Technology to Improve Wellbore Quality during Drilling and Protect Unconventional Reservoirs (Engineering).
Jing, H., He, L., Feng, J., 2019. High strength hydrogels with multiple shape-memory ability based on hydrophobic and electrostatic interactions. Soft Matter 15 (26), 5264–5270.
Karthik, V.P., 2009. Cation-π interactions as a mechanism in technical lignin adsorption to cationic surfaces. Biomacromolecules 4 (10), 798–804.
Korde, J.M., Kandasubramanian, B., 2020. Naturally biomimicked smart shape memory hydrogels for biomedical functions. Chem. Eng. J. 379, 122430.
Li, T., Nudelman, F., Tavacoli, J.W., 2016. Long-lived foams stabilized by a hydrophobic dipeptide hydrogel. Adv. Mater. Interfac. 3 (3), 1500601.
Li, J., Qiu, Z.S., Zhong, H.Y., Zhao, X., Yang, Y.F., Huang, W.A., 2021. Optimizing selection method of continuous particle size distribution for lost circulation by dynamic fracture width evaluation device. J. Petrol. Sci. Eng. 200, 19.
Liu, H., Xiong, C., Tao, Z., 2015. Zwitterionic copolymer-based and hydrogen bonding-strengthened self-healing hydrogel. RSC Adv. 5 (42), 33083–33088.
Magzoub, M.I., Salehi, S., Hussein, I.A., Nasser, M.S., 2020. Loss circulation in drilling and well construction: the significance of applications of crosslinked polymers in wellbore strengthening: a review. J. Petrol. Sci. Eng. 185, 13.
Mohamed, H.G., Aboud, A.A., Abd El-Salam, H.M., 2021. Synthesis and characterization of chitosan/polyacrylamide hydrogel grafted poly(N-methylaniline) for methyl red removal. Int. J. Biol. Macromol. 187, 240–250.
Niamlaem, M., Phuakkong, O., Garrigue, P., 2020. Asymmetric modification of carbon nanotube Arrays with thermoresponsive hydrogel for controlled delivery. ACS Appl. Mater. Interfaces 12 (20), 23378–23387.
Rui, X., Weikai, L., 2020. Research and development of intelligent drilling technology in China. Journal of Northeast Petroleum University 44 (4), 15–21.
Shi, W., Lu, X., Qing, H., 2019. Self-healing behaviors of sulfobetaine polyacrylamide/chromium gel decided by viscosity and chemical compositions. J. Appl. Polym. Sci. 136 (4), 46991.
Sun, T.L., Kurokawa, T., Kuroda, S., Bin Ihsan, A., Akasaki, T., Sato, K., Haque, M.A., Nakajima, T., Gong, J.P., 2013. Physical hydrogels composed of polyampholytes demonstrate high toughness and viscoelasticity. Nat. Mater. 12 (10), 932–937.
Sun, X., Bai, B., Alhuraishawy, A.K., Zhu, D., 2020. Understanding the plugging performance of HPAM-Cr (III) polymer gel for CO2 conformance control. SPE J. 26 (5), 3109–3118.
Syed, A., Pantin, B., Durucan, S., Korre, A., Shi, J.-Q., 2014. The use of polymer-gel solutions for remediation of potential CO2 leakage from storage reservoirs. Energy Proc. 63, 4638–4645.
Vipulanandan, C., Mohammed, A., 2015. Effect of nanoclay on the electrical resistivity and rheological properties of smart and sensing bentonite drilling muds. J. Petrol. Sci. Eng. 130, 86–95.
Wang, L., Long, Y., Ding, H., 2017a. Mechanically robust re-crosslinkable polymeric hydrogels for water management of void space conduits containing reservoirs. Chem. Eng. J. 317, 952–960.
Wang, L.Z., Long, Y.F., Ding, H.F., Geng, J.M., Bai, B.J., 2017b. Mechanically robust re-crosslinkable polymeric hydrogels for water management of void space conduits containing reservoirs. Chem. Eng. J. 317, 952–960.
Wang, Q., Pan, X., Lin, C., 2020. Ultrafast gelling using sulfonated lignin-Fe3+ chelates to produce dynamic crosslinked hydrogel/coating with charming stretchable, conductive, self-healing, and ultraviolet-blocking properties. Chem. Eng. J. 396, 125341.
Xian, S., Webber, M.J., 2020. Temperature-responsive supramolecular hydrogels. J. Mater. Chem. B. 8 (40), 9197–9211.
Xie, B.Q., Ma, J., Wang, Y., Tchameni, A.P., Luo, M.W., Wen, J.T., 2021. Enhanced hydrophobically modified polyacrylamide gel for lost circulation treatment in high temperature drilling. J. Mol. Liq. 325, 11.
Xiong, H., Li, Y., Ye, H., 2020. Self-healing supramolecular hydrogels through host-guest interaction between cyclodextrin and carborane. J. Mater. Chem. B. 8 (45), 10309–10313.
Xu, J., Wang, Z., You, J., 2020. Polymerization of moldable self-healing hydrogel with liquid metal nanodroplets for flexible strain-sensing devices. Chem. Eng. J. 392, 123788.
Xu, C., Yang, X., Liu, C., Kang, Y., Bai, Y., You, Z., 2022. Dynamic fracture width prediction for lost circulation control and formation damage prevention in ultra-deep fractured tight reservoir. Fuel 307, 121770.
Yang, D.Q., Rochette, J.F., Sacher, E., 2005. Spectroscopic evidence for π-π interaction between poly(diallyl dimethylammonium) chloride and multiwalled carbon nanotubes. J. Phys. Chem. B 10 (109), 4481–4484.
Yang, L., Jiang, G., Shi, Y., Lin, X., Yang, X., 2017a. Application of ionic liquid to a high-performance calcium-resistant additive for filtration control of bentonite/water-based drilling fluids. J. Mater. Sci. 52 (11), 6362–6375.
Yang, L., Jiang, G., Shi, Y., Yang, X., 2017b. Application of ionic liquid and polymeric ionic liquid as shale hydration inhibitors. Energy Fuel. 31 (4), 4308–4317.
Yang, E., Fang, Y., Liu, Y., Li, Z., Wu, J., 2020. Research and application of microfoam selective water plugging agent in shallow low-temperature reservoirs. J. Petrol. Sci. Eng. 193, 107354.
Yuk, H., Zhang, T., Lin, S., Parada, G.A., Zhao, X., 2016. Tough bonding of hydrogels to diverse non-porous surfaces. Nat. Mater. 15 (2), 190–196.
Zhang, X., Li, Z., Yang, P., 2021. Polyphenol scaffolds in tissue engineering. Mater. Horiz. 8 (1), 145–167.